CHAPTER 1

The physics of geoneutrinos and their detection

Geoneutrinos are born in β-decays of nuclear isotopes naturally present in the Earth. The geoneutrinos can provide the information on the Earth's interior otherwise hidden from reasearchers. The origin of geoneutrino and techniques for their detection are discussed, primarily the detection through inverse β-decay on protons in liquid scintillator detectors. The expected signals and background for the inverse β-decay detectors are considered. Other possible detection techniques are evaluated in view of the geoneutrino studies.

1.1 Introduction

Geoneutrino is an electron antineutrino accompanying β-decay of nuclear isotopes present in the Earth. Interest in geoneutrino has risen very recently, in parallel with development of large volume detectors, able to detect their tiny fluxes. The main scientific outcomes expected from these measurements are the abundancies and distributions of radioactive elements inside the Earth, beyond the reach of direct measurements by sampling. The natural radioactivity of the Earth is a powerful source of heat, influencing the thermal history of the Earth. The knowledge of the radioactive content of the Earth's depths is essential for many problems in geoscience.

Historically, the first attempt to built the theory of Earth's cooling was developed by lord Kelvin in the middle of the XIX century with aim of calculating the age of the Earth. He calculated the time of conductive cooling of the initially hot molten Earth to be 20-400 millions years. The calculation exhibited huge progress compared to the biblical 6000 years, but still far away from the modern evaluations of 4.5 billion years based on completely different ideas. From the point of view of modern knowledge, Kelvin's calculations contained two errors: he neglected convection inside the Earth, and his model was missing the presence of any heat sources. If the former was an avoidable systematics error of the approach, the latter was connected with a lack of knowledge at that time. In fact, the most powerful modern source of heat, the natural radioactivity, was discovered only half a century later.

The importance of radioactivity in the Earth's heat balance was understood quite early after its discovery. In 1905, Irish physicist J. Joly was the first who turned attention to rock radioactivity as a source of the Earth's thermal

energy. His early calculations showed that the distribution of radioactive elements is not uniform throughout the Earth's volume, as the concentration of radioactive elements in the crust extrapolated to the entire volume would result in significantly higher heat production than the known total heat flux from the Earth. In other words, these calculations indicated that the concentration of radioactive elements in the mantle and core are lower than in the crust [1]. In the 70s, the U and Th concentrations were measured in mantle rock samples extracted from the ocean floor, and they indeed turned out to be low. Thus, natural radioactive isotopes are concentrated mainly in the continental crust. The energy from the decay of radioactive isotopes is an important source of heat in the Earth, it is estimated to account for roughly half of the total Earth's heat release. The Earth emitted more radiogenic heat at the initial stage of its existance than it emits now, primarily because rocks at that time had more radioactive elements. The primary heat source in the early Earth were decays of ^{26}Al isotope with half-life of 0.717 Myr.

There are different types of radioactive decays among the radioactive isotopes heating the Earth. The energy of α-decays is totally converted into the heat, while energy released in β-decays is partially taken away by neutrinos. Historically, the study of β-decay provided the first physical evidence of the neutrino. The continuous spectrum of β-decay was a mystery, as there was no apparent third particle to provide the energy and angular momentum balance. In a famous letter written in 1930, W. Pauli suggested the existence of a light neutral particle, which he called the neutron. This "neutron" emitted during β-decay would account for the missing energy. In 1931 Enrico Fermi renamed the particle to neutrino. The neutrino's interaction with matter is extremely weak, and their detection was an experimental challenge for a quarter of centenary, accomplished only in 1956 through an experiment by F. Reines and C. Cowan [2]. Because each β-decay is accompanied by neutrino emission, detecting neutrinos would mean registering the corresponding β-decays in the Earth depth.

The first mention of geologically produced neutrinos in modern physics can be found in the G. Gamow letter to F. Reines (see i.e. [3]). Gamow suggested that unidentified background observed in the nuclear reactor experiment by F. Reines and C. Cowan (devoted to the neutrino search) could be due to the neutrinos from β-decaying members in the families of U and Th. In his teletype answer F. Reines reported the first estimate of the antineutrino flux of 10^8 cm^{-2}s^{-1} of 1 MeV neutrinos at the Earth's surface based on the heat loss at the surface of 50 erg cm^{-2} s^{-1}, which was not enough to explain the excess (despite of the fact that antineutrino flux was significantly overestimated in this calculation).

In the 60s, G. Eder [4] and G. Marx [5] first pointed out the importance of geoneutrino studies in the context of the problem of heat release in the Earth. At the same time, Russian academician M.A. Markov turned his attention to the possibility of recording geoneutrinos in the reaction of inverse β-decay (IBD) on proton [6]. The modern theoretical study of this problem is dated to the work of L.M. Krauss, S.L. Glashow, and D.N. Schramm [7]. The first paper in a geophysical journal appeared only in the 90s [8]. The potential of Borexino and KamLAND detectors for geoneutrinos was first pointed out in papers [9] and [10]. The interest in geoneutrino in the geoscience community exploded after the first experimental results on their detection from KamLAND [11] and Borexino

collaborations [12]. At present one can state that we are witnessing the formation of a new field of geophysics: neutrino geophysics, merging the fine art of neutrino detection with geophysics.

Geoneutrino flux measurements will give answers on the still debatable questions about the natural radioactivity of our planet: what is the radiogenic contribution to the total heat generated by the Earth; how much uranium and thorium are contained in the Earth's crust and mantle; is there any georeactor or hidden excessive ^{40}K at the center of the Earth, as it is suggested by some theoreticians; and are the geochemical bulk silicate Earth (BSE) models consistent with geoneutrino data?

1.2 Geoneutrino origin

A geoneutrino is an electron (anti)neutrino accompanying the β-decay of nuclear isotopes present in the Earth. The natural radioactivity of the present Earth is associated with long-lived radioactive isotopes (radionuclides) with half-lives of the order of billions of years, comparable with the Earth's and Solar system's age. The complete list of these isotopes (including both α and β radioactive nuclides) contains 29 nuclides, another six nuclides have half-lives longer than 80 million years, long enough for some of them to have survived in noticeable quantities untill present days. These 35 naturally occurring radioactive nuclides comprise the primordial nuclides with different abundancies and life-times, but the major contribution to the Earth radioactivity comes from very few of them, namely from decays of radioactive elements in chains of decays started with ^{238}U and ^{232}Th, and from decays of ^{40}K, with some contribution from ^{235}U chain and from decays of ^{87}Rb.

Electron antineutrinos ($\overline{\nu_e}$) are produced in radioactive β-decays:

$$ {}^{A}_{Z}X \rightarrow {}^{A}_{Z+1}Y + e^{-} + \overline{\nu_e}, $$

where A and Z are the mass and atomic number of the parent nucleus X. Daughter nucleus Y has the same A and Z increased by 1. The mass difference Q_0 between the parent and daughter decay is distributed between the electron and antineutrino, providing continuous electron (and thus correlated with it neutrino) energy spectra. The details of the β- spectra shape calculations can be found in appendix 1.8.1.

The most important decays, from the geophysical point of view, are those in the U and Th decay chains:

$$ {}^{238}_{92}\mathrm{U} \rightarrow {}^{206}_{82}\mathrm{Pb} + 8\alpha + 6e^{-} + 6\overline{\nu_e} + 51.77 \quad \mathrm{MeV}, $$

$$ {}^{235}_{92}\mathrm{U} \rightarrow {}^{207}_{82}\mathrm{Pb} + 7\alpha + 4e + 4\overline{\nu_e} + 46.42 \quad \mathrm{MeV}, $$

$$^{232}_{90}\mathrm{Th} \rightarrow ^{208}_{82}\mathrm{Pb} + 6\alpha + 4e^- + 4\overline{\nu_e} + 42.66 \quad \mathrm{MeV},$$

and two channels of ^{40}K decay (β-decay and electron capture):

$$^{40}_{19}\mathrm{K} \rightarrow ^{40}_{20}\mathrm{Ca} + e^- + \overline{\nu_e} + 1.311 \quad \mathrm{MeV}, \quad (89.3\%),$$

$$^{40}_{19}\mathrm{K} + e^- \rightarrow ^{40}_{18}\mathrm{Ar} + \nu_e + 1.505 \quad \mathrm{MeV}, \quad (10.7\%).$$

Neutrinos are produced only in electron capture of ^{40}K: in contrast to the Sun powered by nuclear fusion, Earth "shines" essentially in antineutrinos produced in radioactive β^--decay. The last decay of some importance is that of ^{87}Rb. Rb is the 23d most abundant element in nature, so despite of its relatively low specific heat yield it could be important in precision calculations:

$$^{87}_{37}\mathrm{Rb} \rightarrow ^{87}_{38}\mathrm{Sr} + e^- + \overline{\nu_e} + 0.2833 \quad \mathrm{MeV}.$$

Abundances and main characteristics of the three decay chains and 2 isotopes, providing the overwhelming contribution to the Earth's radiogenic heating, together with the characteristics of accompanying neutrinos/antineutrinos are summarized in Table 1.1. The details of the calculations are summarized in Tables 1.2-1.4. The main route of the decay chains are presented schematically in Fig. 1.3 and Fig. 1.4. The less important branches are excluded in these charts for the sake of simplicity (all the minor details can be found in tables). As a result of very low cross section of interaction with matter, neutrinos carry away a fraction of the energy release in β-decays and only the remaining energy from electrons and gammas is converted to heat (compare Q_{tot} and Q_{eff} columns of the tables).

The uranium chain (historically called the "radium series") begins with naturally occurring ^{238}U. It includes isotopes of astatine, bismuth, lead, polonium, protactinium, radium, radon, thallium, and thorium, providing that all are present in any uranium- containing sample. The total energy released per one decay of ^{238}U to ^{206}Pb is 51.8 MeV in assumption of secular equilibrium. The properties of individual decays of the ^{238}U decay chain are summarized in Table 1.2.

Another chain is started with the less abundant uranium isotope, ^{235}U ("actinium series"). This decay series includes isotopes of actinium, astatine, bismuth, francium, lead, polonium, protactinium, radium, radon, thallium, and thorium. The total energy released per one decay of parent ^{235}U to ^{207}Pb is 46.4 MeV in assumption of secular equilibrium. The properties of individual decays of ^{235}U chain are summarized in Table 1.3.

Natural uranium, along with ^{238}U and ^{235}U, contains the decay product ^{234}U, which is in secular equilibrium

	Units	^{238}U	^{235}U	^{232}Th	^{40}K		^{87}Rb
					β (89.3%)	EC (10.7%)	
Natural isotopic abundance		0.992742	0.007204	1.0000	$1.17(1)\cdot10^{-4}$		0.2783
Life-time, $T_{1/2}$	Gy	4.468	0.7038	14.0	1.248		47.5
Isotope atomic mass	g/mol	238.051	235.044	232.038	39.9640		86.909
Total decay energy, $Q_{\rm tot}$	MeV	51.77±0.02	46.42±0.01	42.66±0.01	1.311	1.505	0.283
Heating energy, $Q_{\rm H}$	MeV	47.71±0.02	44.41±0.01	40.44±0.01	0.589	1.461	0.122
Specific heat, ϵ_ν	μW·kg^{-1}	94.5±0.1	4.2	26.4	$2.58\cdot10^{-3}$	$0.77\cdot10^{-3}$	$1.7\cdot10^{-2}$
Specific antineutrino luminosity,$\epsilon_{\rm H}$	kg^{-1}s^{-1}	$7.41\cdot10^{7}$	$2.3\cdot10^{6}$	$1.63\cdot10^{7}$	$2.73\cdot10^{4}$	0	$8.9\cdot10^{5}$

Table 1.1: Main contributors to the radiogenic heat production. $Q_{\rm tot}$ is total energy released in corresponding decay/chain of decays including the energy lost to neutrinos (evaluated using the last up to date version of ENSDF database [?], the errors are calculated using the data of the same database). $Q_{\rm H}$ is "visible" (dissipated for heating) energy release, namely the total energy released excluding the energy lost to neutrinos.ϵ_ν and $\epsilon_{\rm H}$ are specific neutrino luminosity and heat production respectively, per 1 kg of mass of naturally occurring element, taking into account the natural abundance of corresponding radioactive isotope fraction.

with its parent ^{238}U, and its long life time provides 0.000055 isotopic abundance in natural uranium. ^{234}U and its daughter decays are included in the calculations as a part of the parent ^{238}U chain.

The last chain considered is the "thorium series" beginning with naturally occurring ^{232}Th. This series includes isotopes of actinium, bismuth, lead, polonium, radium, and radon. The total energy released from ^{232}Th to ^{208}Pb is 42.6 MeV. The properties of individual decays of the ^{238}U chain are summarized in Table 1.4.

The data for the evaluation of energy release were taken from the last available version of ENSDF database [1]. It should be noted that while $Q_{\rm tot}$ is based on the measured values with typical errors below 0.1%, the precision of evaluation of $Q_{\rm eff}$ depends on many unknown factors, including precision of measurement of branching ratios for complex decays (with β-decay into excited levels of daughter nuclei) and shapes of β-decays. The universal β-decay shape is used in calculations with the exception of ^{210}Bi in the ^{238}U chain and ^{40}K β-decay (3rd forbidden). As an example of possible error, the $Q_{\rm eff}$ value estimated with universal shape would be 0.397 (compared to 0.318 MeV) for ^{210}Bi β-decay and 0.509 MeV instead of 0.589 MeV for ^{40}K. The total error on energy release is not influenced significantly by this fact, as only a small fraction of total energy is released in β-decays (4.0 out of 47.7 MeV in ^{238}U chain; 1.2 out of 44.4 MeV in ^{235}U chain; 2.3 out of 40.4 MeV in ^{232}Th chain).

The antineutrino spectra, normalized to one decay of the parent nucleus, are shown in Fig.1.1.

For a given amount of radioactive isotopes, the energy released in radioactive decays is strictly connected to the amount of antineutrinos produced in these decays. The total neutrino production rate (or luminosity) L_ν can be related to the mass of radioactive isotopes contained in the Earth using the data from Table 1.1:

$L_\nu = [7.64 \cdot {\rm M(U)} + 1.63 \cdot {\rm M(Th)} + 2.7 \cdot 10^{-3} \cdot {\rm M(K)} + ...] \cdot 10^{24} s^{-1}$.

A similar relation between radiogenic heat production $H_{\rm R}$ and the mass of radioactive isotopes can be expressed as:

$H_R = [9.87 \cdot {\rm M(U)} + 2.64 \cdot {\rm M(Th)} + 3.34 \cdot 10^{-4} \cdot {\rm M(K)} + ...] \cdot {\rm TW}$,

[1] Evaluated Nuclear Structure Data File (ENSDF), last updated 2014-09-09. The ENSDF database contains evaluated nuclear structure and decay information for over 3000 nuclides. Continuously updated with new evaluations published in Nuclear Data Sheets; we used the database version from april 2014 : https://www-nds.iaea.org/ensdf_base_files/

Isotope	Historic name	Decay mode	Branching %	$T_{1/2}$	Daughter	Q keV	Q_{eff} keV	rate 1/Bq	Q_{eff}/Bq
^{238}U	Uranium I (U_I)	α	100	4.468 Gy	^{234}Th	4270(3)	4270	1.000	4270
^{234}Th	Uranium X_1(UX_1)	β^-	100	24.10 d	^{234m}Pa	273(3)	158	1.000	158
^{234m}Pa	Uranium X_2(UX_2)	IT	0.16(4)	1.159 m	^{234}Pa	79(5)	79	1.6e-3	0
		β^-	99.84(4)		^{234}U	2267(4)	812	0.9984	811
^{234}Pa	Uranium Z (UZ)	β^-	100	6.70 h	^{234}U	2195(4)	1747	1.6e-3	3
^{234}U	Uranium II (U_{II})	α	100	$2.455{\cdot}10^5$ y	^{230}Th	4860(1)	4860	1.000	4860
^{230}Th	Ionium (Io)	α	100	$7.54{\cdot}10^4$ y	^{226}Ra	4770(2)	4770	1.000	4770
^{226}Ra	Radium (Ra)	α	100	$1.6{\cdot}10^3$ y	^{222}Rn	4871(0)	4871	1.000	4871
^{222}Rn	Radon (Rn)	α	100	3.8235 d	^{218}Po	5590(0)	5590	1.000	5590
^{218}Po	Radium A (RaA)	β^-	0.020	3.098 min	^{218}At	260(12)	80	2e-4	0
		α	99.980		^{214}Pb	6115(0)	6115	0.9998	6114
^{218}At		β^-	0.1	1.5 s	^{218}Rn	2881(3)	1117	2e-7	0
		α	99.9		^{214}Bi	6874(0)	6874	2e-4	0
^{218}Rn		α	100	35 ms	^{214}Po	7263(2)	7263	2e-7	0
^{214}Pb	Radium B (RaB)	β^-	100	26.8 min	^{214}Bi	1019(11)	529	0.9998	529
^{214}Bi	Radium C (RaC)	β^-	99.979	19.9 min	^{214}Po	3270(11)	2142	0.9998	2141
		α	0.021		^{210}Tl	5617(1)	5617	2.1e-4	1
^{214}Po	Radium C' (RaC')	α	100	164.3 μs	^{210}Pb	7833(0)	7833	0.9998	7832
^{210}Tl	Radium C" (RaC")	β^-	100	1.30 min	^{210}Pb	5490(12)	3624	2.1e-4	1
^{210}Pb	Radium D (RaD)	β^-	100	22.20 y	^{210}Bi	65(1)	46	1.000	46
		α	$1.9{\cdot}10^{-6}$		^{206}Hg	3792(20)	3792	1.9e-8	0
^{210}Bi	Radium E (RaE)	β^-	100%	5.012 d	^{210}Po	1162(1)	310	1.000	310
		α	$1.32{\cdot}10^{-4}$		^{206}Tl	5036(1)	5036	1.32e-6	0
^{210}Po	Radium F (RaF)	α	100	138.376 d	^{206}Pb	5408(0)	5408	1.000	5408
^{206}Hg		β^-	100	8.32 min	^{206}Tl	1308(20)	527	1.9e-8	0
^{206}Tl	Radium E" (RaE")	β^-	100	4.202 min	^{206}Pb	1532(1)	541	1.32e-6	0
^{206}Pb	Radium G (RaG)			stable					

Table 1.2: ^{238}U chain. Q is total energy released in corresponding decay including the energy lost to neutrinos rounded to keV, corresponding error is quoted in parenthesis after each Q value, also rounded to 1 keV. Q_{eff} is effective energy release, the total energy release excluding the energy lost to neutrinos. Rate is given per 1 Bq of parent decay, the last column contains effective energy release per 1 Bq of parent decay.

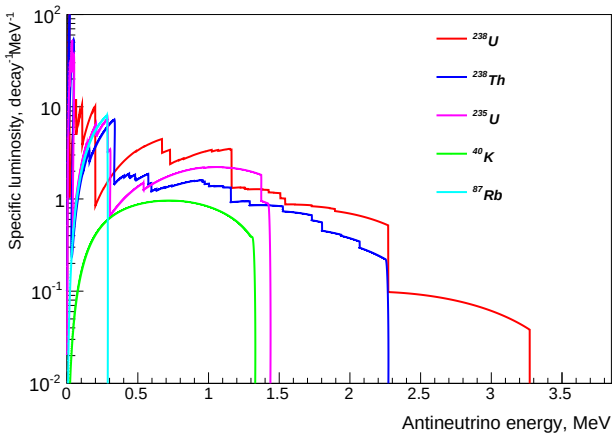

Figure 1.1: Specific antineutrino energy spectra (normalized to one decay of the parent nucleus)

Isotope	Historic name	Decay mode	Branching %	$T_{1/2}$	Daughter	Q MeV	Q_{eff} MeV	rate 1/Bq	Q_{eff}/Bq
^{235}U	Actin Uranium (AcU) Actino-Uranium	α	100	0.704 Gy	^{231}Th	4678(1)	4678	1.000	4678
^{231}Th	Uranium Y (UY)	β^-	100	25.52 h	^{231}Pa	392(2)	189	1.000	189
^{231}Pa	Protoactinium	α	100	$3.276{\cdot}10^4$ y	^{227}Ac	5150(1)	5150	1.000	5150
^{227}Ac	Actinium (Ac)	β^-	98.62	21.772 y	^{227}Th	45(1)	17	0.9862	16
		α	1.38		^{223}Fr	5042(0)	5042	0.0138	70
^{227}Th	Radioactinium (RdAc)	α	100	18.68 d	^{223}Ra	6147(0)	6147	0.9862	6062
^{223}Fr	Actinium K (AcK)	β^-	99.994	22.0 min	^{223}Ra	1149(1)	434	0.0138	6
		α	0.006		^{219}At	5562(3)	5562	$8.3{\cdot}10^{-7}$	0
^{223}Ra	Actinium X (AcX)	α	100	11.43 d	^{219}Rn	5979(0)	5979	1.000	5979
^{219}At		α	97	56 s	^{215}Bi	6324(15)	6324	$8.0{\cdot}10^{-7}$	0
		β^-	3		^{219}Rn	1566(3)		$2.5{\cdot}10^{-8}$	0
^{219}Rn	Actinon (An) Actinium emanation	α	100	3.96 s	^{215}Po	6946(0)	6946	1.000	6946
^{215}Bi		β^-	100	7.6 min	^{215}Po	2189(15)	1054	$8.0{\cdot}10^{-7}$	0
^{215}Po	Actinium A (AcA)	α	99.99977	1.781 ms	^{211}Pb	7526(1)	7526	1.000	7526
		β^-	$2.3{\cdot}10^{-4}$		^{215}At	0.715		$2.3{\cdot}10^{-6}$	0.000
^{211}Pb	Actinium B (AcB)	β^-	100	36.1 min	^{211}Bi	1367(6)	515	1.000	515
^{215}At		α	100	0.10 ms	^{211}Bi	8178(4)	8178	$2.3{\cdot}10^{-6}$	0
^{211}Bi	Actinium C (AcC)	α	99.724	2.14 min	^{207}Tl	6750(1)	6750	0.99724	6732
		β^-	0.276		^{211}Po	574(5)	174	$2.76{\cdot}10^{-3}$	0
^{207}Tl	Actinium C" (AcC")	β^-	100	4.77 min	^{207}Pb	1418(5)	495	0.99724	495
^{211}Po	Actinium C' (AcC)	α	100	0.516 s	^{207}Pb	7594(1)	7594	$2.76{\cdot}10^{-3}$	21
^{207}Pb	Actinium D			stable					

Table 1.3: ^{235}U chain

Isotope	Historic name	Decay mode	Branching %	$T_{1/2}$	Daughter	Q keV	Q_{eff} keV	1/Bq	Q_{eff}/Bq
^{232}Th	Uranium X1 (UX_1)	α	100	$1.40{\cdot}10^{10}$ y	^{228}Ra	4082(1)	4082	1	4082
^{228}Ra	Mesothorium I ($MsTh_1$)	β^-	100	5.75 y	^{228}Ac	46(1)	25	1	25
^{228}Ac	Mesothorium II ($MsTh_2$)	β^-	100	6.15 h	^{228}Th	2134(3)	1398	1	1379
^{228}Th	Radiothorium (RdTh)	α	100	1.9116 y	^{224}Ra	5520(0)	5520	1	5520
^{224}Ra	Thorium X	α	100	3.66 d	^{220}Rn	5789(0)	5789	1	5789
^{220}Rn	Thoron (Tn) Thorium Emanation (ThEm)	α	100	55.6 s	^{216}Po	6405(0)	6405	1	6405
^{216}Po	Thorium A (Th A)	α	100	0.145 s	^{212}Pb	6906(1)	6906	1	6906
^{212}Pb	Thorium B (Th B)	β^-	100	10.64 h	^{212}Bi	0.570(2)	0.320	1	0.320
^{212}Bi	Thorium C (Th C)	α	35.94	60.55 min	^{208}Tl	6207(0)	6207	0.3594	2.231
		β^-	64.06		^{212}Po	2252(2)	933	0.6406	598
^{212}Po	Thorium C' (Th C')	α	100	0.299 μs	^{208}Pb	8954	8954	0.6406	5736
^{208}Tl	Thorium C" (Th C")	β^-	100	3.053 min	^{208}Pb	4999(2)	3980	0.3594	1.431
^{208}Pb	Thorium D (Th D)	stable							

Table 1.4: ^{232}Th chain

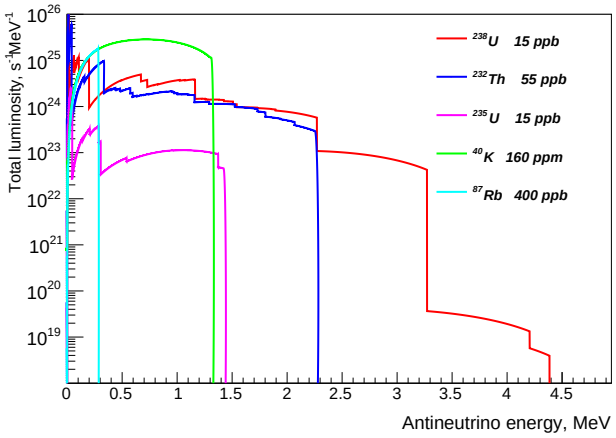

Figure 1.2: Total antineutrino differential luminosities, the abundances from [13] used in calculation are shown after each isotope notation.

where masses of corresponding elements are in units of 10^{17} kg, 1 TW is 10^{12} W.

Radiogenic heat and primordial heat of the Earth constitutes two main contributions to the total energy loss of the Earth. Insignificant amount of heat is produced due to tidal effects, chemical differentiation, crystallization in the D" layer etc. These less important sources produce no more than one percent of the total. The ratio of the radiogenic heat production to the total is called the Urey ratio and is an important quantity characterizing heat production in the Earth.

The differential total antineutrino luminosities of the Earth ($\frac{dL_\nu(E)}{dE}$), calculated used abundances of natural isotopes in the Earth from [13], are shown in Fig.1.2.

There is no way to directly measure the heat flow from the radiogenic sources. The most recent evaluation using the the available geothermal data gives the total heat flow of 47±2 TW [14]. Additionally, there is no way to measure the total antineutrino luminosity, as it would require 4π coverage of the whole Earth. Modern large volume neutrino detectors offer an opportunity to measure antineutrino flux in two geographical positions: at the Gran Sasso mountain massif in Central Italy (where the Borexino detector is installed) and in the Kamioka mine in Japan (hosting the KamLAND detector).

The total luminosity L_ν and related heat production H_R can be estimated using the values of geoneutrino flux measured by the antineutrino detector.

The geoneutrino flux measured by a neutrino detector at certain position depends on the distribution of radioactive isotopes in the Earth bulk, and varies within an order of magnitude for different locations on the Earth's surface. One should take into account neutrino oscillations when comparing the expected neutrino flux with the measured one.

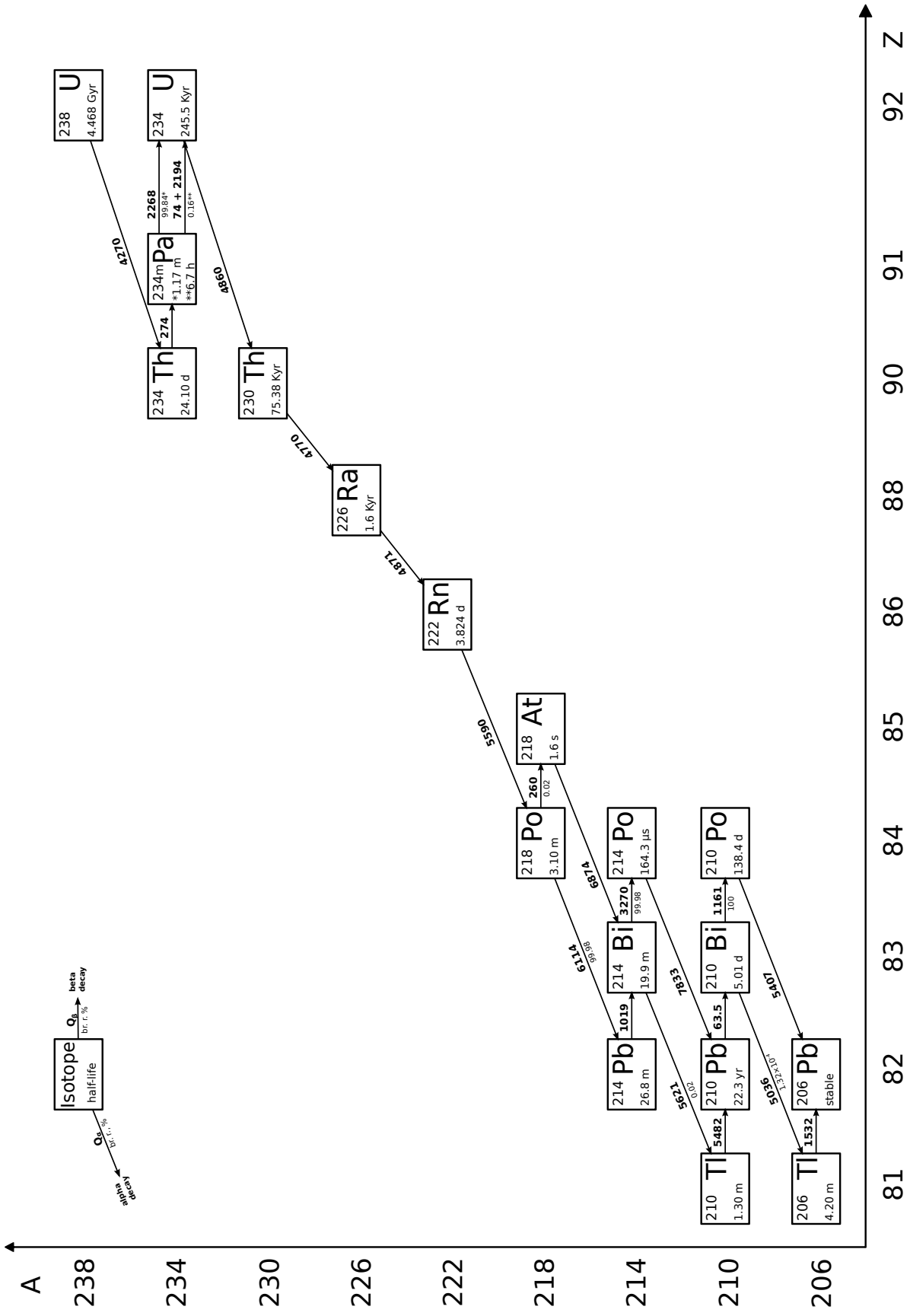

Figure 1.3: ^{238}U decay chain

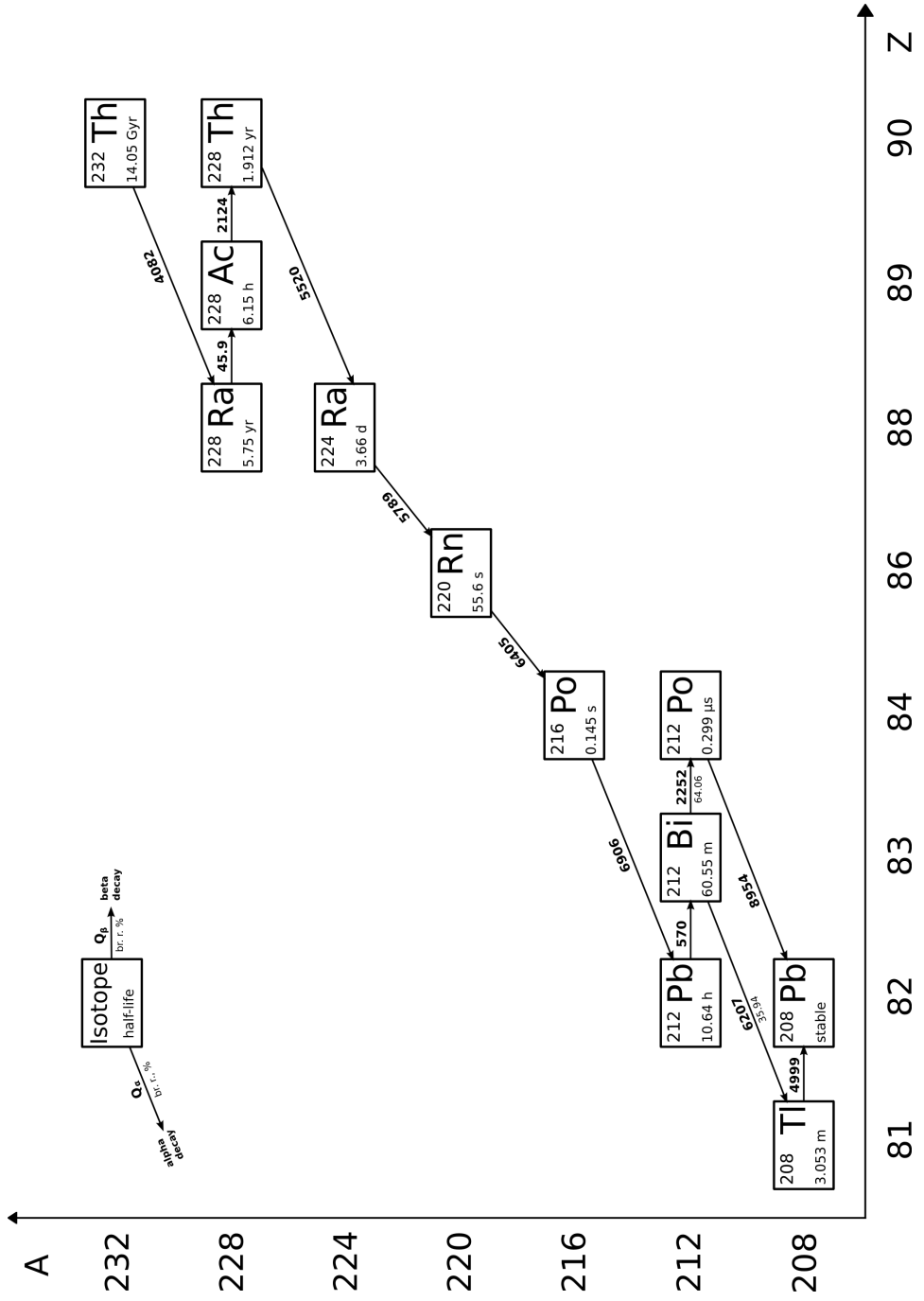

Figure 1.4: ^{232}Th decay chain

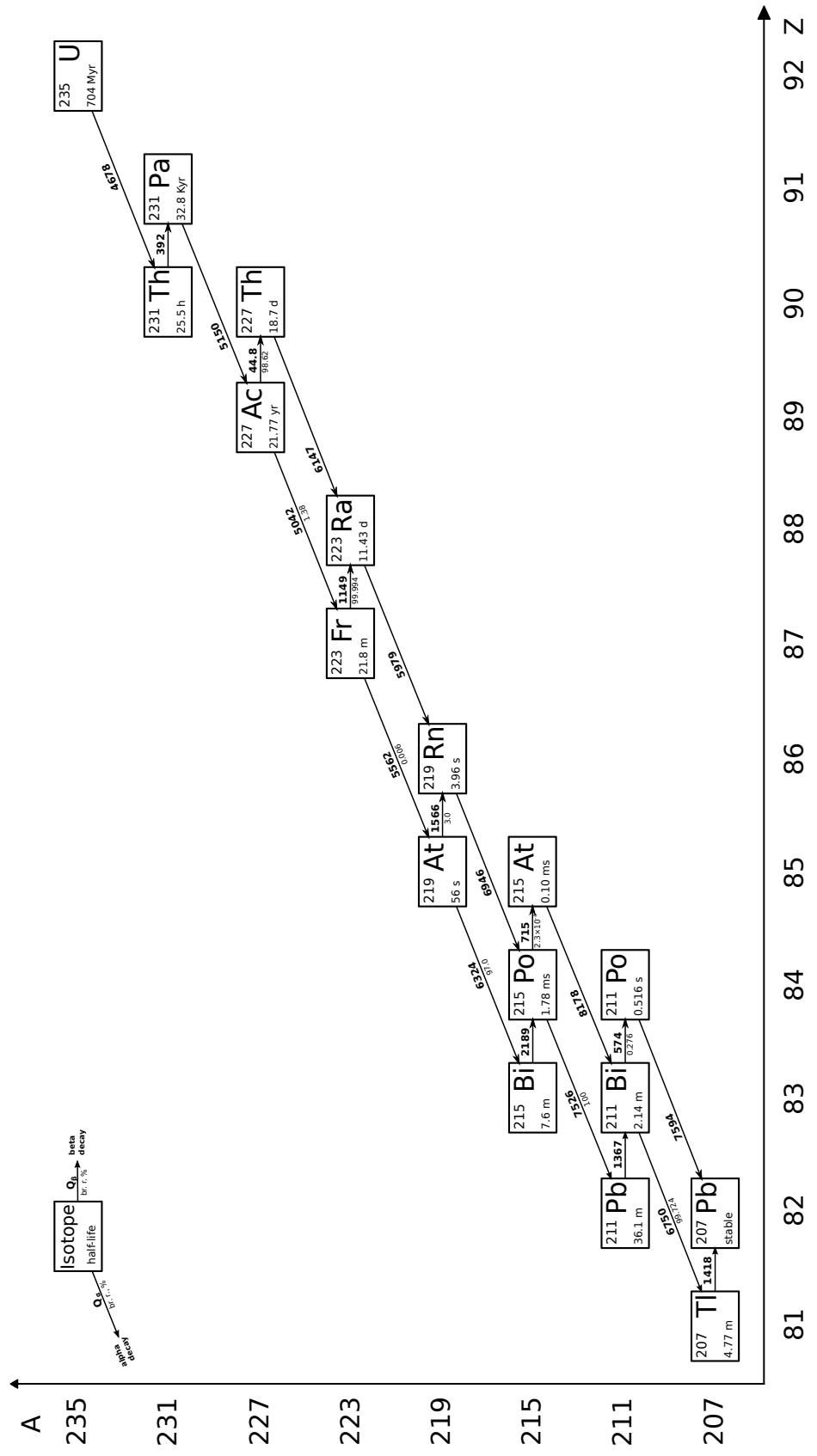

Figure 1.5: ^{235}U decay chain

1.3 Geoneutrino flux and neutrino oscillations

Differential neutrino flux at the detector's location can be calculated by integrating the antineutrino flux from all possible points of origin in the Earth, taking into account neutrino oscillations and summing over all contributing β-decays:

$$\phi_I(E_\nu) = \int_V \frac{\rho(\overrightarrow{r})}{4\pi|\overrightarrow{R_D} - \overrightarrow{r}|^2} \cdot n_I(E_\nu) \cdot A_I(\overrightarrow{r}) \cdot P_{ee}(E_\nu, |\overrightarrow{R_D} - \overrightarrow{r}|) d\overrightarrow{r}, \tag{1.1}$$

where index I={U,Th} denotes U or Th chain (because of the 1.81 MeV threshold of the IBD neutrino detectors only β-decaying isotopes with end-point energy $E_0 > 1.81$ MeV are involved in the summation), $\rho(\overrightarrow{r})$ is the Earth density at position $\overrightarrow{r}$, $n_I(E_\nu)$ is neutrino energy spectrum in the corresponding chain normalized to the number of neutrinos emitted in the chain ($\int n_{Th}(E)dE$ =4, $\int n_U(E)dE$ =6), $\overrightarrow{R_D}$ is position of the detector, integration is performed over Earth's volume V, and $P_{ee}(E, r)$ is electron antineutrino survival probability for antineutrino energy E at distance r from the neutrino source. $A_I(\overrightarrow{r})$ is the specific activity of the chain I at the position with coordinates $\overrightarrow{r}$:

$$A_I(\overrightarrow{r}) = \frac{a_I(\overrightarrow{r}) \cdot C_I}{\tau_I m_I}, \tag{1.2}$$

where $a_I(\overrightarrow{r})$ is the mass abundance of the corresponding parent element, C_I, τ_I, and m_I are correspondingly isotopic abundance, life-time, and atomic mass of isotope.

The electron neutrino survival probability appears in equation (1.1) because the cross section of interactions of neutrinos with the active media of the detector depends on the neutrino flavour. All existing neutrino oscillation data (with a few exceptions indicating the presence of the fourth hypothetical sterile neutrino, a case which will not be discussed here) can be described assuming a 3-flavour neutrino mixing in vacuum. Mass eigenstates correspond to the mass states of neutrinos, called ν_1, ν_2 and ν_3. It follows from experimental data that neutrinos must be light with $m_1, m_2, m_3 \ll 1$ eV, and all three must have different masses to allow for oscillations. The usual flavour states produced in nuclear reactions are the mixture of the mass states, the composition of which can change as neutrino propagates. We can state that, at present, all of the properties of the mixing matrix, describing neutrino mixing, are rather well established with respect to the precision needed in geoneutrino flux estimations. The electron antineutrino, being born in β-decay as a mass state mixture corresponding to the electron flavour, after traveling a distance $|\overrightarrow{R_D} - \overrightarrow{r}|$ will change its flavour properties. The distant observer will still detect these neutrinos in electron flavour with a (survival) probability P_{ee}, while the complementary probability 1-P_{ee} remains for observing other neutrino flavours. If a detector is unable to register non-electron neutrino flavours, the factor P_{ee} should be applied to obtain the electron flavour component. In the general case (i.e. in the case of a hypothetical detector sensitive to the neutrino elastic scattering) one should also take into account the presence of other flavour components.

The three-flavour electron neutrino survival probability is

$$P_{ee}^{3\nu}(E_\nu, L) = 1 - \left(\cos^4\Theta_{13}\sin^2 2\Theta_{12}\cdot\Delta_{21} + \sin^2 2\Theta_{13}\left[\cos^2 2\Theta_{12}\cdot\Delta_{31} + \sin^2 2\Theta_{12}\cdot\Delta_{32}\right]\right), \tag{1.3}$$

where Θ_{12} and Θ_{23} are mixing angles, and Δ_{ij} is defined as:

$$\Delta_{ij} = \sin^2\left(1.27|\Delta m_{ij}|[eV^2]\frac{L[m]}{E_\nu[MeV]}\right), \tag{1.4}$$

with $\Delta m_{ij} = m_i^2 - m_j^2$, the neutrino eigenstate mass squared difference. Note that by definition we have only two independent mass squared differences because $\Delta m_{31}^2 = \Delta m_{32}^2 + \Delta m_{21}^2$. The values of Δm_{21}^2 and Δm_{31}^2 are measured in oscillation experiments providing that one of the two independent mass squared differences, say Δm_{21}^2, is much smaller in absolute value than the second one $|\Delta m_{21}^2| \ll |\Delta m_{32}^2|$, providing $\Delta m_{31}^2 \approx \Delta m_{32}^2$. The data imply: $\Delta m_{21}^2 \simeq 7.6\cdot 10^{-5}$ eV^2 and $\Delta m_{31}^2 \simeq 2.4\cdot 10^{-3}$ eV^2.

Formula (1.3) is quite simple and can be used directly in precise calculations.

The survival probability can be approximated using fast oscillations for energies in the range of interest (1.8-3 MeV). Indeed, the length of oscillations for Δm_{12}^2 is of the order of 100 km and for Δm_{23}^2 is even lower. Both are small compared to the Earth radius of 6400 km and the average survival probability is:

$$\left\langle \mathrm{P}_{\mathrm{ee}}^{3\nu}(E_\nu, L)\right\rangle = 1 - 0.5\left(\cos^4\Theta_{13}\sin^2 2\Theta_{12} + \sin^2 2\Theta_{13}\right). \tag{1.5}$$

Using the values of $\sin^2\Theta_{13} = 0.096 \pm 0.013$ and $\sin^2 2\Theta_{12} = 0.306^{+0.018}_{-0.015}$ we obtain for the electron antineutrino survival probability:

$$\langle \mathrm{P}_{\mathrm{ee}}\rangle = 0.548^{+0.012}_{-0.013}, \tag{1.6}$$

which can be used in calculations instead of (1.3).

All calculations above are performed for the case of the so called vacuum oscillations, in the absence of matter. While traveling through dense matter (in our case through the Earth) the mixing angles acquire a density-dependent matter term. In fact, the electron neutrino/antineutrino interacts through charged and neutral currents with electrons of media, while those of other flavours interact through neutral currents only. As a result, a difference in the potential of interaction for electronic and other flavours appears, $2G_F n_e$, where n_e is the electron density. The electron density in the Earth varies. The changes in density are especially noticeable at the boundaries of different layers of Earth. The survival probabilities have been calculated numerically solving equations of motion in [15]. It was concluded that the matter effect increases the survival probability by $\sim$2% and the spectral distortions are below 1%.

1.4 Geoneutrino detection

The physics of antineutrino detection is basically the same in both detectors, exploiting the inverse β-decay (IBD) reaction on a proton:

$$\overline{\nu_e} + p \rightarrow n + e^+. \tag{1.7}$$

It was first applied in the pioneering research of F. Reinis and C.L. Cowan who conducted the first experiment on reactor antineutrino detection. Liquid organic scintillators can be used as detection media, as it is rich in free protons and cheap, permitting construction of large detectors. At present, geoneutrino observations have been reported by two collaborations with Borexino and KamLAND liquid scintillator detectors respectively.

The reaction has kinematic threshold of 1.806 MeV ($E_{th} = \frac{(m_n+m_e)^2-m_p^2}{2m_p} = 1.806$ MeV), excluding the lower energies antineutrino detection in inverse β-decay detectors. The energy of the incoming antineutrino E_ν is strongly correlated with the energy of the positron, created as a result of the interaction. The positron takes away the energy $E_{kin} = E_\nu - 1.806$ MeV in the form of the kinetic energy, with a negligible fraction of this excess energy left for the kinetic energy of the neutron. The kinetic energy of the positron is transformed into scintillation light detected by photosensitive elements of the detector - photomultiplier tubes (PMTs). The annihilation of the positron produces two gamma-quanta of 0.511 MeV energy each, also producing light flashes in the scintillator through Compton electrons. Thus, the total amount of scintillation light corresponds to the visible energy of:

$$E_{vis} = E_{kin} + 2m_e = E_\nu - 0.8 \text{ MeV}. \tag{1.8}$$

Together with the positron, a neutron is released in reaction (1.7). This gives one an opportunity to "tag" the reaction, looking for pairs of events correlated in space and time. Indeed, the neutron is thermalized very effectively in proton-rich media (in 10-20 collisions with protons), and the thermal neutron has relatively high cross section of interaction with protons. It is captured on the proton with a typical time of 200-250 μs in liquid organic scintillators, releasing easily- detectable energetic gamma quantum:

$$n + p \rightarrow D + \gamma(2.2 \text{ MeV}). \tag{1.9}$$

In large volume detectors all 2.2 MeV of energy is lost in Compton scattering on electrons and thus converted into light, and the gamma is effectively detected. In such a way, the "tag" is provided by 2.2 MeV "delayed" event in a time coincidence with a "prompt" one. The time window defining the "true" coincidence can be chosen on the basis of the expected accidental coincidence rate and the life-time of the neutron with respect to the capture on proton. The tagging technique allows for effective reduction of random coincidences background. Further improvement of the technique can be achieved due to the possibility of event vertex reconstruction offered by modern large volume

liquid scintillator (LS) detectors equipped with many photosensors. The position is reconstructed using the arrival times of photons at each photosensor (for more details and examples of the technique see i.e. [16, 17, 15]). The position reconstruction is essential for reducing the background from the construction materials in the active volume of the scintillator. The LS is contained in a transparent vessel, and its material is unavoidably less purified from the radioactive impurities compared to the LS. The inner section of the LS volume (fiducial volume) provides the best signal-to-background ratio and is selected using position reconstruction code. In such a way, the remaining outer section serves as an active shielding for the fiducial volume. Because two events in reactions (1.7) and (1.9) occur at the same position (the typical drift of a neutron is some centimeters compared to ten centimeters of the typical position reconstruction precision), another condition on the pair of events can be applied: their positions should be reconstructed as close to each other as possible. The selection criteria could be set based on the balance of the efficiency of the spatial cut (defined by the precision of the reconstruction algorithm) and on the accidental coincidence rate surviving the applied cut. An example of the selection criteria tuning for two experiments can be found in chapters dedicated to Borexino and KamLAND experiments in this volume.

Compared to the low energy (few MeV range) neutrino detection, the antineutrino detection is relatively easier due to the possibility of using the delayed coincidence tag and due to the fact that antineutrino detection reaction (1.7) for these energies has higher cross section than the reaction of neutrino elastic scattering used in neutrino detectors. Of course, the geoneutrino (antineutrino) elastic scattering will contribute to the total untagged event counting rate, but it is small compared to the natural background from elastic scattering of neutrinos. The total cross section for reaction (1.7) can be written in the low energy approximation as [19]:

$$\sigma_n \simeq \frac{2\pi^2}{m_e^5 \cdot f(1+\delta_R) \cdot \tau_n} E_e p_e, \tag{1.10}$$

where $E_e = E_\nu - (m_n - m_p) = E_\nu - 1.293$ MeV is the positron energy and p_e is the corresponding momentum, both measured in MeV, τ_n is the life-time of the neutron and $f(1+\delta_R) = 1.71480$ is a theoretical phase-space factor. The numerical factor before $E_e p_e$ in (1.11) depends inversely on the neutron decay time; using a recent value of $\tau_n = 880.3 \pm 1.1$ ns [20] we obtain:

$$\sigma_n \simeq 9.57 \cdot 10^{-44} p_e E_e \; cm^2. \tag{1.11}$$

The relatively small corrections of the order of E_ν/m_p and α/π can be accurately evaluated if necessary (see [21]). In this way the cross section of the inverse β-decay can be evaluated with an accuracy of $\sim$0.2%. The experimental errors are an order of magnitude larger (1.4-3.0% [22]).

The differential geoneutrino event rate at the detector is:

$$\frac{dN}{dE_\nu} = N_p \sigma_n(E_\nu) \epsilon(E_\nu) \phi(E_\nu),$$

Isotope	Bq/Bq[Th]	$I \pm \delta I$	Q, MeV	Type	S,TNU	f_{Th},%	f_{tot},%
^{228}Ac$\rightarrow$ ^{228}Th	1.000	0.07±0.05	2.0663	Allowed ($3^+ \rightarrow 2^+$)	0.3	4.8	0.8
^{228}Ac$\rightarrow$ ^{228}Th	1.000	0.006±0.005	1.9374	Allowed ($3^+ \rightarrow 4^+$)	0.0	0.1	0.0
^{212}Bi$\rightarrow^{212}$Po	0.6406	0.5537±0.0011	2.252026	1-st forbidden ($1^{(-)} \rightarrow 0^+$)	6.4/7.4	95.1	16.0

Table 1.5: Properties of β-decays in the ^{232}Th chain contributing to geoneutrino signal in IBD detectors. The second column contains activity of the corresponding reaction with respect to the activity of parent ^{232}Th. The $I \pm \delta I$ contains the relative intensity of the corresponding decay (with respect to one parent decay) with associated experimental error. Q is the β-decay end-point. S is signal at the detector position measured in TNU in assumption of 10^6 cm^{-2}s^{-1} total neutrino flux (from ^{238}U and ^{232}Th chains only) at the detector distributed between U and Th in accordance to the chondritic ratio and in assumption of the universal (allowed) shape; alternative values (separated by a slash) are calculated in accordance with the decay type. f_{Th} and f_{tot} denote the fraction of the signal in the ^{232}Th chain and in total geoneutrino signal correspondingly in assumption of the allowed shapes. When calculating the values of the last column, the chondritic ratio of 3.9 for Th/U masses was assumed.

Isotope	Bq/Bq[U]	$I_k \pm \delta I_k$	Q, MeV	Type	S,TNU	f_U,%	f_{tot},%
^{234m}Pa$\rightarrow^{234}$U	0.9984	0.9757±0.002	2.269	1-st forbidden ($0^- \rightarrow 0^+$)	13.0/14.6	38.4	31.9
^{214}Bi$\rightarrow^{214}$Po	0.99979	0.1910±0.0017	3.270	1-st forbidden ($1^- \rightarrow 0^+$)	20.6/22.3	60.8	50.6
		0.0058±0.0018	2.661	1-st forbidden ($1^- \rightarrow 2^+$)	0.2/0.3	0.7	0.6
		0.0735±0.0005	1.892	1-st forbidden ($1^- \rightarrow 2^+$)	0.1/0.1	0.1	0.1
		0.0089±0.0003	1.855	1-st forbidden ($1^- \rightarrow 0^+$)	0.0	0.0	0.0

Table 1.6: Properties of β-decays in ^{238}U chain contributing to geoneutrino signal in IBD detectors. The notations are the same of Table 1.5.

where N_p is the number of target protons within the fiducial volume of the detector, $\epsilon(E_\nu)$ is detection efficiency, and $\phi(E_\nu)$ is differential electron antineutrino flux at the detector's location.

1.5 Expected geoneutrino signal in IBD antineutrino detector

A convenient unit to describe the rate of interactions in IBD detectors is Terrestrial Neutrino Unit (TNU) corresponding to 1 interaction for 10^{32} target protons in one year: 10^{32} target protons are contained in roughly 1 kton of typical liquid organic scintillator, and few years is a typical expected exposure time for geoneutrino detection. Thus, a count in TNU units roughly corresponds to the expected event rate per year in 1 kt scale IBD detector.

Because of the reaction threshold, the detection of antineutrinos from decays of ^{40}K and ^{87}Rb is impossible with IBD detectors. The same applies to all of the β-decays in the ^{235}U chain and most of the β-decays in the ^{238}U and ^{232}Th chains.

Only two isotopes in each chain have enough energetic β-decays to provide a contribution to the IBD signal. In the ^{232}Th decay chain these are two branches of ^{228}Ac decay (into ground state and to the first excited one), and decay of ^{212}Bi into the ground state. In the ^{238}U chain these are the decays of ^{234m}Pa and 4 branches of the ^{214}Bi decay. The properties of β-decays in the ^{232}Th and ^{238}U chains contributing to geoneutrino signal are presented in Tables 1.5 and 1.6, respectively. The corresponding neutrino spectra for U and Th are shown in Fig.1.6. The total neutrino spectrum calculated for chondritic ratio for Th/U masses (M(Th)/M(U)=3.9) is shown in Fig.1.7.

As one can see from Table 1.5, the contribution from ^{228}Ac is quite uncertain. It is contributing 0.6% in the

total antineutrino signal uncertainty, because of the poorly measured relative intensity of the decay. Decay of ^{214}Bi into the ground state contributes another 0.4% into the total error of the signal. Summed quadratically, these two contributions constitute 0.7%, and other transitions in both decay chains do not contribute significantly to the total signal uncertainty. The uncertainty of the β-decay shape can, in principle, contribute much more to the signal uncertainty. The values after slashes in the S column of the tables are calculated in assumption of the β-decay shape in accordance with decay type (mostly first forbidden) and can serve as an estimation of (maximum) systematics associated with unknown precise shapes of the decay. One can see that these errors can contribute up to 10% into the signal. These errors cannot be summed quadratically because of the unknown correlations; all can contribute in the same direction. Any deviation from the allowed shape towards the forbidden one will increase the total signal. There are good qualitative reasons to assume the allowed shape for these β-decays, as discussed in [3] (see chapter 1.8.1). At any rate, the quantitative estimation of the corresponding errors is quite complicated. It is clear that only precise experiments can provide proper shapes. The most important fraction of β-spectra to be investigated, from the point of view of geoneutrino signal calculations, lays in its low-energy region, the most difficult region to access in experimental studies (because of the detector threshold and increase of backgrounds at low energies).

An attempt to measure the shape of the ^{214}Bi $\beta + \gamma$ decay was reported in [23]. The feeding probability of the lowest state of ^{214}Bi, providing the most important contribution for geoneutrino signal, was found to be $p_0 = 0.177 \pm 0.004$ under the assumption of universal neutrino spectrum shape, consistent with the indirect estimate of the table of isotopes[2]. Larger statistics and reduction of systematics should allow for the testing of possible distortions of the neutrino spectrum from that predicted using the universal shape [23]. It was found that the effect of uncertainties on the geoneutrino signal is mostly negligible: in the fit of the ^{214}Bi decay data with the completely unconstrained shape parameter, p_0 and p_1 (feeding probabilities to the ground and the first excited states, the only one giving a contribution above 1.81 MeV) the effects of changes of shape and of p_0 on the signal are anticorrelated, if the spectrum is deformed such that there are more (less) low-energy electrons, the corresponding best-fit value for p_0 is lower (higher). While the values of p_0 range from 0.13 to 0.20, the signal changed only by about $\pm 2\%$., i.e. the resulting signal is weakly dependent on the spectral shape [23].

Expected total spectrum corresponding to chondritic ratio of M(Th)/M(U)=3.9 is shown in Fig. 1.7.

The principal factors responsible for uncertainty of the expected geoneutrino signal (or related radiogenic heat) are the ones in masses and spatial distribution of radioactive isotopes in the Earth. Series of geological models are developed with a wide range of predicted radiogenic heat. Thus, the measurement of geoneutrino flux will allow to discriminate among the Earth models. Other uncertainties of the expected geoneutrino signal are less important (including uncertainty in the oscillation parameters, uncertainties of the β-decay shapes, uncertainties in the branching ratios etc.) because they are still beyond the sensitivity of the experiments. It should be noted that due to the fact that main contributors to the geoneutrino signal (U, Th, and K) have similar geochemical properties

[2] the consistency was checked against the value $p_0 = 0.182 \pm 0.006$ from [24], updated data [?] gives $p_0 = 0.1910 \pm 0.0017$ that is 3.2σ away from the measured. This could indeed indicate the deviations from the allowed universal shape.

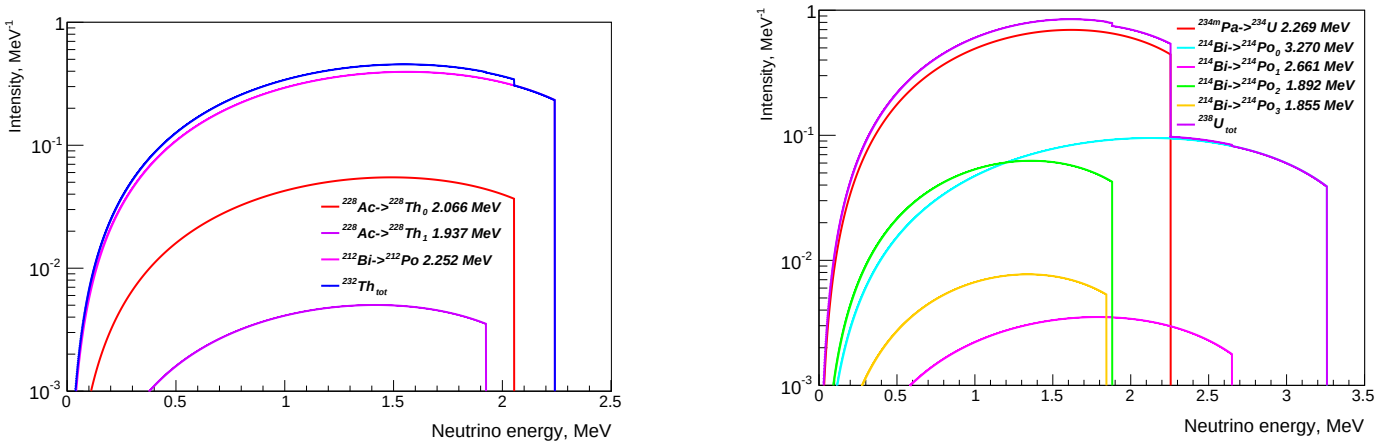

Figure 1.6: Neutrino spectra for β-decaying isotopes in ^{232}Th and ^{238}U chains with end-point energy $E_0 > 1.806$ MeV. Resulting total spectra are normalized to one parent decay.

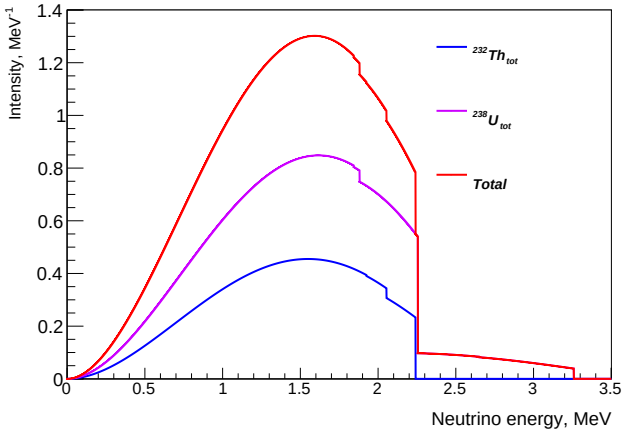

Figure 1.7: Resulting neutrino spectra for ^{232}Th and ^{238}U chains from isotopes with end-point energy $E_0 > 1.806$ MeV and their sum for chondritic Th/U ratio (Th/U=3.9). Total spectrum is normalized to unity.

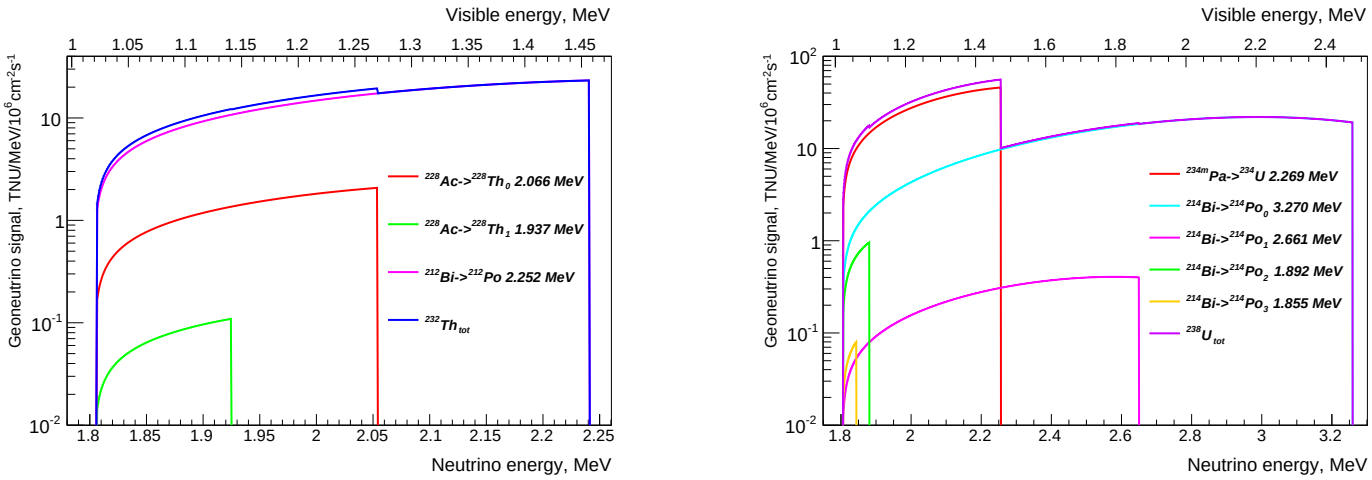

Figure 1.8: Expected IBD neutrino signal from decays in ^{232}Th and ^{238}U chains (incident antineutrino flux of 10^6 cm^{-2}s^{-1} is assumed in calculations)

(all are lithophile elements), their content in different Earth reservoirs is positively correlated. In contrary, the total mass constraint of the Bulk Silicate Earth model anti-correlates these element abundances in complementary reservoirs. The problem of the uncertainties and correlations in geoneutrino fluxes calculation was considered in [25]. Authors constructed a "geoneutrino source model" (GNSM) for the U, Th, and K abundances in the main Earth reservoirs, and then used it to make geoneutrino signal predictions. They showed also how future data can constrain the error matrix of the model itself. It should be noted however that present experimental uncertainties (connected mainly with low statistics) appear to be significantly larger than the GNSM ones.

1.6 Backgrounds in IBD detectors and their suppression

Experimental errors in geoneutrino experiments are associated mainly with low statistics and with the presence of backgrounds, as it is very difficult to ensure a background-free environment for counting such rare events. Principal contributions to background come either from antineutrino sources other than geoneutrinos (reactor antineutrinos) or from events mimicking antineutrino interactions. The latter can be produced by cosmic muons (cosmogenic background) or by intrinsic residual radioactive contamination of LS (internal background). Other natural antineutrino sources such as diffuse flux of neutrino from past supernovae (supernova relic neutrinos, the flux is ~ 10 cm^{-2}s^{-1} [26]) and atmospheric neutrinos (~ 1 cm^{-2}s^{-1} [27]) are negligible compared to the geoneutrino flux ($\sim 10^6$ cm^{-2}s^{-1}) and do not contribute to the background.

Reactor antineutrino. Untill now the geoneutrino flux measurement was a by-product result of other studies (Solar neutrino fluxes in the case of Borexino, with an average distance to the reactors of ~ 1000 km and reactor antineutrino flux studies at the ~ 180 km distance from reactors in the case of KamLAND), and reducing background from reactors was not an option to tune in the projects. The reactor antineutrino flux depends on the power of

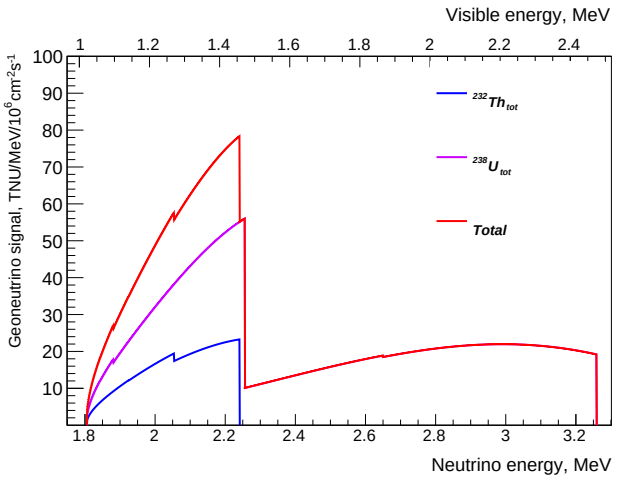

Figure 1.9: Expected IBD neutrino signal from decays in ^{232}Th and ^{238}U chains and total signal. Chondritic ratio of Th/U=3.9 and incident antineutrino flux of 10^6 cm^{-2}s^{-1} are assumed in calculations.

nuclear reactors and on the distance between the reactors and the detector. Keeping track of power history of near reactors helps in statistical extraction of the expected signal.

The next generation antineutrino detectors sensitive to the neutrino hierarchy (i.e. 20 kton JUNO [28]) are being planned at a distance of ∼60 km from reactors, making antineutrino background even stronger than in the case of KamLAND detector (with average distance to the reactors ∼180 km). On the other hand, these detectors will provide higher statistics of events, in principle allowing for the use of statistical separation of geo- and reactor neutrinos on the basis of directionality.

Average shift of neutrons in the direction of incoming antineutrinos has been observed by reactor experiments (i.e. by CHOOZ collaboration [29]). More recent theoretical considerations with respect to the geoneutrino detection can be found in [30]. The basic idea is to search for the statistical displacement of the neutron with respect to the prompt event ($\overrightarrow{\Delta R} = \overrightarrow{R_{prompt}} - \overrightarrow{R_{delayed}}$). The displacement of the emitted positron is negligible and can't provide any reasonable information regarding the direction of incoming antineutrino. In contrast, the neutron is emitted in a relatively narrow range (below ∼55 degrees [30]) of angles around the direction of the antineutrino with energies up to 100 keV for reactor antineutrinos. The emitted neutron is slowed down in the proton- rich media, the average angle in single collision is $\overline{\cos\Theta_n} = \frac{2}{3A}$. In scattering on protons (atomic number A=1) neutron preserves maximum directionality possible. The slow down occurs very quickly, the displacement from the production point is determined by the first few scatterings, still preserving the initial direction. The later isotropic diffusion process does not change the average displacement, which in the case of CHOOZ was observed to be 1.7 cm.

Whether such a displacemt can be observed depends on the precision of position reconstruction and on the statistics of events involved in analysis. If we consider realistic case of 10 cm position reconstruction precision, we need at least 100 events in order to be able to separate 1 cm at 1 σ C.L. Directionality can also help to separate the crust and mantle components of the total geoneutrino flux.

Cosmogenic background. Muons produced in primary cosmic ray interactions in atmosphere penetrate deep underground. Though the cosmic muon flux is significantly reduced in the underground labs, the flux of muons is still high enough to provide significant background. The site depth is the main factor influencing the cosmic muon flux, which decreases exponentially with depth. Among existing underground sites the best shielding against cosmic muons is provided in SNO laboratory (Canada) placed in a 2 km deep mine and providing shielding equivalent to 6010 meters of water. Baksan laboratory in the Caucasus mountains (Russia) provides 4800 m of water equivalent (m.w.e.) shielding. The LNGS laboratory in Italy, where Borexino detector is placed, provides 3400 m.w.e. shielding; the KamLAND site is less protected (2700 m.w.e.), and the future JUNO site will be even less protected (2000 m.w.e.) against cosmic muons.

The most dangerous cosmogenic background is associated with neutron-rich isotopes produced by spallation. Some of these isotopes are long-lived and can decay with emission of neutron, and thus perfectly mimick the antineutrino signal. These are long-lived ^{8}He ($T_{1/2} = 119.1$ ms, $\beta+n$ branching ratio of 16%) and ^{9}Li ($T_{1/2} = 178.3$ ms, $\beta+n$ branching ratio of 50.8%). Because $\beta+n$ decays are indistinguishable from antineutrino events, the only way to suppress the corresponding background is complete or partial exclusion of events after an identified muon passing through the detector. In the first case all events in the detector's volume are excluded from the analysis in the time window of the order of 1-2 seconds after muon, the veto time can be optimized to provide the best trade between the cosmogenic background reduction efficiency and loss of the live time. In the case of partial veto, only the cylindrical volume around the muon track, where spallation is possible, is excluded from the analysis. This helps to gain in live time, but is more complex as it needs the reconstruction of the muon rack.

Thus the IBD detector should be equipped with a high efficiency muon detector. The criteria for the muon veto depends on the site depth, both the KamLAND and Borexino succeed in reducing this background to negligible values.

Another cosmic muon related background is caused by fast neutrons, produced outside the detector (i.e., by muons not identified by the muon detector). Fast neutrons have a long free path, entering into the detector from outside, and can produce a high energy prompt event, and then thermalize and capture onto a proton, producing an antineutrino-like false event. The amount of these events depends on the site depth and detector (main and muon) geometry, and typically is comparable to the residual background from the $\beta+n$ isotopes. The prompt signal due to the proton scattered off neutron should in principle be distinguishable from signal induced by a positron in LS due to the different timing characteristics of the scintillation flight (a heavy particle produces flashes with stronger "slow" component), allowing for partial discrimination of this background.

Intrinsic backgrounds. Selection criteria for the pairs of correlated events (the so called antineutrino candidate events) are constructed using reconstructed distance ΔR between two events, the time difference between events ΔT, cuts on events energy and cuts on interaction types, if detector provides a possibility to distinguish events caused by β or γ particle and those caused by heavier ones, alphas and/or protons. Because of the presence

of residual radioactivity in LS some false events can be selected after applying the cuts, forming the so called random coincidences background. Their spectra and counting rate can be easily reproduced based on the single (uncorrelated) event spectra, picking pairs of events in an off-time coincidence window (one random and another one from the time window far above the one used to search for the candidates) and applying the same selection criteria used to select candidate events. The overall rate of random coincidences depends quadratically on the single events counts, i.e. on residual radioactivity.

Another source of background is (α, n) reaction on ^{13}C, naturally present in organic scintillator with isotopic abundance of 1.3%. Monoenergetic α-particles with 5.3 MeV kinetic energy are produced in decays of ^{210}Po from the ^{238}U decay chain [31]. In both Borexino and KamLAND detectors the activity of ^{210}Po was found to be higher than what was expected in secular equilibrium with ^{238}U. More details can be found in sections dedicated to Borexino and KamLAND experiments.

Background from radioactive contamination of LS (random coincidences background and background from (α, n) reaction on ^{13}C) can be reduced by choosing better LS purification strategies, as was demonstrated by the Borexino collaboration. Background from radioactive contamination of LS can be further reduced by applying e^+/e^- discrimination method [32], first applied by the Borexino collaboration to reduce background from β^+-decay of cosmogenic ^{11}C [33]. The idea of the method is based on the difference in photon emission temporal distribution. In 50% of cases the decay of positron occurs through a bound orthopositronium state, which delays positron decay in LS by few nanoseconds. This turns out to be enough to be used in statistical positron tagging. In the simple case of other backgrounds to be pure electronic (β-decays), the amount of these events should correspond to the difference between the amount of electron-like and positron-like events, giving additional information for the background suppression.

1.7 Other detection methods

1.7.1 Water based IBD detectors

Water is inexpensive proton-rich media, that would be of a great benefit to use in constructing extra-large geoneutrino detectors. Pure water is being used i.e. in large volume (50 kton) Cherenkov detector Super-Kamiokande [34] to study high-energy part of solar neutrino spectrum. The detector registers electrons scattered by solar neutrinos. Directionality of Cherenkov light is used to suppress backgrounds. Because of the low light yield the energy threshold in water Cherenkov detectors is typically too high (above 3.5 MeV) to detect correlated pairs of events caused by geoneutrinos. An advanced study of neutron tagging in a water Cherenkov detector was reported by the Super-Kamiokande collaboration [35]. The tagging efficiencies of thermal neutrons was evaluated in a 0.2% GdCl3-water solution, and in pure water. They were determined to be 66.7% and 20%, respectively for events above 3 MeV with corresponding background probabilities of 2×10^{-4} and 3×10^{-2}. This is still not enough to

challenge the detection of antineutrino events in the energy range of interest for geoneutrino studies.

The amount of light produced by Cherenkov radiation is 50 times lower than in liquid scintillators and a significant fraction of light is emitted in the UV region, where water is losing transparency and PMTs are not sensitive. Adding a wavelength shifter to water helps to register photons otherwise invisible to PMTs, increasing the amount of detected light by a factor 2-3 [36],[37]. These studies were performed in a view of improving the sensitivity of existing water Cherenkov detectors not aimed at geoneutrino studies. Adding chemicals to water can reduce transparency, which influences the sensitivity.

A more promising approach of using water-based liquid scintillator (WbLS) has been recently discussed in [38]. WbLS is a novel scintillation medium for large liquid detectors, in which scintillating organic molecules and water are co-mixed using surfactants [39]. The possible mixture extends from pure water to pure scintillator, offering a great possibility of tuning the detection media to fit the physics program. Compounds with low content of LS will work in a regime close to that of the water Cherenkov detectors, but offering higher light yield. In contrast, liquid scintillator detectors with the addition of water will gain directionality and metal-loading capability. A variety of solvents are available. In addition, different wavelength shifters and other additives can be used to adjust the timing properties of the final mixture.

The development of WbLS with low attenuation length will allow the construction of large-volume multipurpose detectors, suitable for geoneutrinos studies.

1.7.2 IBD and resonant electron capture on other nuclear targets

Both reactions, in view of geoneutrino detection, have been discussed in early papers [7, 8]. A list of possible nuclear targets can be found in Table 2 of [8]. In general, the majority of considered targets will need huge quantities of material, orders of magnitude more than in the case of detectors exploiting IBD on protons, to provide a comparable counting rate. The lowest energy threshold of 1.041 MeV is provided by a ^{3}He target. This would allow for the detection of antineutrinos from ^{40}K. Unfortunately, the necessary amount of ^{3}He is beyond modern capabilities.

A previously unidentified low-threshold stable target isotope^{106}Cd was proposed in [40]. The natural abundance of ^{106}Cd is very low, 1.25%, and enrichment is needed. A cadmium- tungstate ($CdWO_4$) solid state 200 g detector with enrichment of 66% in ^{106}Cd is available for tests [41]. Detection reaction is IBD on cadmium:

$$\overline{\nu_e} + ^{106}\mathrm{Cd} \rightarrow ^{106}\mathrm{Ag} + e^+. \tag{1.12}$$

The energy threshold of the reaction is 1.216 MeV, below the end-point of ^{40}K β-spectrum (1.311 MeV). The full positron energy is in the $1.02 - 1.12$ MeV energy range. The unstable isotope of silver ^{106}Ag decays into a stable palladium ^{106}Pd with a half- life of 24 min through two concurrent processes, in 37% of cases it decays through

electron capture (EC) "invisible" to the detector :

$$^{106}\mathrm{Ag} + e^- \rightarrow ^{106}\mathrm{Pd} + \nu_e,$$

and in 63% of cases through β^+-decay:

$$^{106}\mathrm{Ag} \rightarrow ^{106}\mathrm{Pd} + e^+ + \nu_e.$$

The coincidence of 511 keV gammas produced in inverse β-decay of cadmium to silver followed by another 511 keV gamma produced by ^{106}Ag β^+-decay provides a tag for antineutrino events. The clear disadvantage of this method is the large delay (corresponding to 24 min half-life) between these two correlated events. But at the same time, the spatial separation is extremely small. Therefore, the spatial coincidence can be used to reject background [42].

1.7.3 Coherent neutrino scattering on nuclei

Detection of low- energy neutrinos via coherent scattering off a nuclear target $\nu + A \rightarrow \nu + A$ remains a sought-after goal in modern neutrino physics. After the discovery of neutral-current neutrino reactions, it became clear that coherent neutrino-nucleus elastic scattering should exist with a cross section quadratic in the weak charge of the nucleus. Coherent scattering occurs by exchange of Z_0-boson between a neutrino and all nucleons of a nucleus, and does not depend on the neutrino flavour. The total cross section for this process is [43]:

$$\sigma = \frac{G^2 N^2}{4\pi} E^2, \tag{1.13}$$

where N is the number of neutrons in the target nucleus. The average energy of the recoil nucleus with mass number A is

$$\overline{E_A} = \frac{2}{3A} E^2, \tag{1.14}$$

here neutrino energy E is measured in MeV and the resulting recoil energy is expressed in keV. For a MeV range neutrino average nucleus recoil energy is few hundreds of an eV for heavy nuclei. To detect such a low recoil energy one needs a detector with very low threshold.

Expressed in units convenient for calculations, the total cross section is:

$$\sigma \simeq 0.42 \cdot 10^{-44} \mathrm{N}^2 \mathrm{E}_\nu^2 \ \mathrm{cm}^2. \tag{1.15}$$

Comparison of cross sections for coherent scattering of neutrino on nucleus of Ge with IBD on protons and

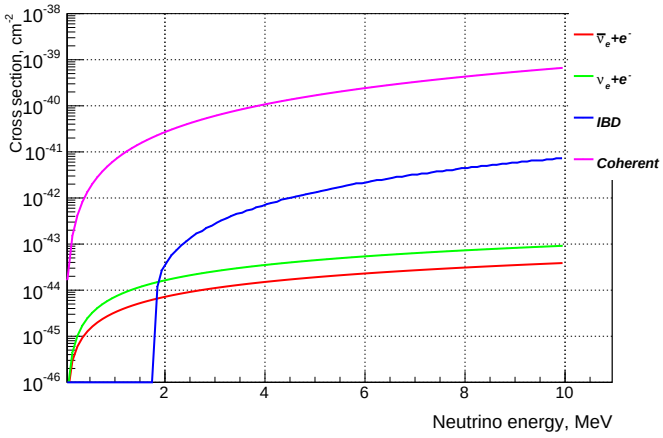

Figure 1.10: Neutrino cross sections for different detection reactions.

elastic scattering for neutrino and antineutrino is presented in Fig. 1.10. One can see that this cross section is significantly higher compared to elastic scattering or IBD on protons.

The coherent scattering is especially important from a practical point of view as massive detectors are usually required for neutrino detection in this energy region due to the small probability of interaction via all other channels. The large coherent scattering enhancement of the cross-section for the coherent scattering process results in significant reduction in size and mass of the relevant neutrino detector. Therefore, developing a technology for detection of neutrinos through the coherent scattering is one of the priorities for neutrino physics. The use of this technique for the geoneutrino studies is questionable, though the absence of threshold makes it very attractive as it is sensitive to the ^{40}K, ^{235}U, and ^{87}Rb geoneutrinos, unreachable in IBD detectors. The main problem here is the presence of much stronger flux of solar neutrinos, representing an irreducible background.

1.7.4 Elastic scattering on electrons

There is no energy threshold for the antineutrino elastic scattering process:

$$\overline{\nu_e} + e^- \rightarrow \overline{\nu_e} + e^-,$$

potentially providing sensitivity to the low energy part of the geoneutrino spectra. The elastic scattering of neutrinos on electrons was successfully used in water Cherenkov (SuperKamiokaNDE, SNO) and liquid scintillator detectors (Borexino) to detect solar neutrinos. The cross-section of antineutrino elastic scattering is 2-3 times lower compared to neutrino scattering (see Fig. 1.10) and the flux of geoneutrinos is 2-4 orders of magnitude lower compared to that of solar neutrinos. Thus, the use of this process for the geoneutrino studies is challenging. The directionality of the scattered electron offers a potential opportunity to suppress neutrino background. The method

is being successfully used in water Cherenkov detectors at higher energies. At present, there are no detectors with directional sensitivity at geoneutrino energies.

The use of this technique for geoneutrino studies will meet the same problem of irreducible solar neutrino background, as in the case of coherent neutrino scattering off nuclei.

1.8 Appendix

1.8.1 Beta spectrum and neutrino spectra

For the allowed β-decays with massless neutrino, the energy spectrum of electrons has the following theoretical ("universal") shape [44]:

$$dN_\beta(w, w_0) = \frac{1}{N_0} F(w, Z_D) C(w) p w (w_0 - w)^2 dw, \tag{1.16}$$

where w and p are the full energy of the electron and its momentum ($p = \sqrt{w^2 - 1}$), respectively. w_0 is the β-decay end-point, and all measured in units $m = h = c = 1$.

$F(w, Z_D)$ is the Fermi function describing correction on screening by atomic electrons in nuclear Coulomb field, with Z_D - charge of the daughter nucleus, and $C(w)$ describes departures from allowed shape. Omitting energy-independent contributions, relativistic Fermi function $F(w, Z_D)$ could be expressed as:

$$F(w, Z_D) = p^{2(\gamma-1)} e^{\pi y} |\Gamma(\gamma + iy)|^2, \tag{1.17}$$

where Γ is complex gamma-function, and$\gamma = \sqrt{1 - (\alpha Z_D)^2}$, $y = 2\pi\alpha Z_D \frac{w}{p}$, andα is fine structure constant.

Normalization factor N_0 is calculated to provide the normalization to unity:

$$\int_1^{w_0} N_\beta(w, w_0) dw = 1. \tag{1.18}$$

The correction of the β-decay spectrum due to the electron screening can be easily taken into account substituting $F(w, Z_D)$ with (Rose correction):

$$F(w - v_0, Z_D) \sqrt{\frac{(w - v_0)^2 - 1}{w^2 - 1}} \frac{w - v_0}{w}, \tag{1.19}$$

where $v_0 \simeq 1.13\alpha^2 Z^{4/3}$. The correction is important for the low energy part of β- spectrum, i.e. relatively important for the neutrino spectra calculation. Another correction is due to the finite nuclear size (negligible for allowed transitions) and a radiative correction due to internal bremsstrahlung (negligible for the low w_0 β-decays). Both were neglected in our calculations of energy release in β-decays of isotopes from U and Th decay chains, and ^{40}K.

The β-decays can involve transitions to excited nuclear states "i" with different branching ratios b_i (with $\sum_i b_i = 1$). Transition to excited states are typical accompanied by energy relaxation involving single gamma or gammas cascade, and/or less abundant conversion electrons.

The most of important contribution to the geoneutrino spectra arises from parity forbidden decays, for which $C(w)$ should be included in calculations. As noted in [3], experimental spectra for forbidden decays of high-Z nuclei show very similar behaviour to the allowed shape. These decays are dominated by momentum-independent matrix elements or by matrix elements with momentum corresponding to electron momentum with $pR \simeq Z\alpha$ (close to the nucleus), weakly dependent on the emerging momentum. This provides a good reason to set $C(w) = 1$ in (1.16). The approximation, in the general case, leads to an error in the estimations and need to be checked.

The shapes of the $\beta-$ spectra have been little studied experimentally since the late 1970s. These spectra were thought to be known accurately enough. Theoretical studies stopped in the 1980's. However, at present, it could be stated that not enough data are available, especially for high forbidding orders and at low energy [45]. The precise knowledge of the shape of energy spectra and their uncertainties, especially in the low-energy region of the $\beta-$spectrum, are needed for precise geoneutrino flux estimations. The same concerns the feeding probabilities in complex decay schemes.

Bibliography

[1] J. Joly, "Radioactivity and geology, an account of the influence of radioactive energy on terrestrial history", New York, D. van Nostrand (1909).

[2] C. L. Cowan Jr., F. Reines, F. B. Harrison, H. W. Kruse, and A. D. McGuire, Science **124,** 103-104 (1956).

[3] G. Fiorentini, M. Lissia, F. Mantovani, " Geoneutrinos and Earth interior", Phys.Reports **453**, 117 (2007).

[4] G. Eder, Nucl.Phys., **78**, 657 (1966).

[5] G. Marx, Czech.J.Phys. **19**, 1471 (1969).

[6] M. Markov, "Neutrino", Nauka, Moscow (1964).

[7] L. M. Krauss, S. L. Glashow, and D. N. Shramm, "Antineutrino astronomy and geophysics", Nature **310**, 191 (1984).

[8] M. Kobayashi and Y. Fukao, "The Earth as an antineutrino star", Geophysical Research Letters, **18**, 633-636 (1991).

[9] R. S. Raghavan, et al., "Measuring the Global Radioactivity in the Earth by Multidetector Antineutrino Spectroscopy", Phys.Rev.Lett. **80**, 635 (1998).

[10] C. G. Rothschild, M. Chen, F. P. Calaprice, "Antineutrino Geophysics with Liquid Scintillator Detectors", Geophys.Res.Lett. **25**, 1083 (1998).

[11] T. Araki, et al., "Experimental investigation of geologically produced antineutrinos with KamLAND", Nature **436**, 499 (2005).

[12] G. Bellinii, et al., "Observation of geo-neutrinos", Phys. Lett. B **687**, 299 (2010).

[13] W. F. McDonough, "Earth's Core", Encyclopedia of Geochemistry, Kluwer Academic Publishers, 151- 156 (1999).

[14] J. H. Davies and D. R. Davies, "Earth's surface heat flux", Solid Earth, **1**, 5-24 (2010).

[15] S. Enomoto, "Neutrino Geophysics and Observation of Geo-Neutrinos at KamLAND," Ph. D. Thesis, Tohoku University, Japan (2005).

[16] O. Smirnov, "Energy and Spatial Resolution of a Large-Volume Liquid-Scintillator Detector", Instruments and Experimental Techniques **46** 327-344 (2003).

[17] G. Bellini, et al., "Final results of Borexino Phase-I on low-energy solar neutrino spectroscopy", Phys. Rev. **D 89**, 112007 (2014).

[18] A. Strumia, F. Vissani, "Precise quasielastic neutrino/nucleon cross-section", Physics Letters **B 564**, 42–54 (2003).

[19] A. Formaggio and G. P. Zeller, "From eV to EeV: Neutrino cross sections across energy scales", Rev. Mod. Phys. **84**, 1307 (2012).

[20] K. A. Olive et al. (Particle Data Group), Chin. Phys. **C38**, 090001 (2014) (URL: http://pdg.lbl.gov).

[21] P. Vogel and J. F. Beacom, "Angular distribution of neutron inverse beta decay, $\overline{\nu_e} + p \to e^+ + n$", Phys. Rev. **D 60**, 053003 (1999); A. Kurylov, M. J. Ramsey-Musolf and P. Vogel, "Radiative corrections to low-energy neutrino reactions", Phys.Rev. **C 67**, 035502 (2003).

[22] G. Zacek et al., "Neutrino-oscillation experiments at the Gösgen nuclear power reactor", PRD **34**, 2621 (1986); G. S. Vidyakin et al. "Limitations on the characteristics of neutrino oscillations", JETP Lett. **59**, 390-393 (1994); Y. Declais et al, "Study of reactor antineutrino interaction with proton at Bugey nuclear power plant", Phys. Letters **338**, 383 (1994).

[23] G. Fiorentini, A. Ianni, G. Korga, M. Lissia, F. Mantovani, L. Miramonti, L. Oberauer, M. Obolensky, O. Smirnov, and Yu. Suvorov, "Nuclear physics for geo-neutrino studies", Phys.Rev. **C81,** 034602 (2010).

[24] Y. A. Alkovali, "Nuclear Data Sheets for A=214", Nucl. Data Sheets **76**, 127 (1995).

[25] G. L. Fogli, E. Lisi, A. Palazzo and A. M. Rotunno, "Geo-Neutrinos: A Systematic Approach to Uncertainties and Correlations". Earth, Moon, and Planets, 111–130 (2006).

[26] S. Ando, "Cosmic Star Formation History and the Future Observation of Supernova Relic Neutrinos", The Astrophysical Journal, **607**, 20-31 (2004).

[27] T. K. Gaisser and M. Honda, "Flux of atmospheric neutrinos", Annual Review of Nuclear and Particle Science **52**, 53-199 (2002).

[28] T. Adam et al, "JUNO Conceptual Design Report", arXiv:1508.07166 (2015).

[29] M. Apollonio, et al., "Determination of neutrino incoming direction in the CHOOZ experiment and its application to supernova explosion location by scintillator detectors", Phys.Rev. **D 61,** 012001 (2000).

[30] M. Batygov, "On the Possibility of Directional Analysis for Geo-neutrinos". Earth, Moon, and Planets, 183–192 (2006).

[31] S. Harissopulos, H. W. Becker, J. W. Hammer, A. Lagoyannis, C. Rolfs, and F. Strieder, "Cross section of the ^{13}C(α,n)^{16}O reaction: A background for the measurement of geo-neutrinos", Phys.Rev. **C 72**, 062801 (2005)

[32] D. Franco, G. Consolati, and D. Trezzi, "Positronium signature in organic liquid scintillators for neutrino experiments", Phys. Rev. **C 83**, 015504 (2011).

[33] G. Bellini, et al., "First Evidence of pep Solar Neutrinos by Direct Detection in Borexino", Phys.Rev.Letters **108**, 051302 (2012).

[34] K. Abe et al., "Solar neutrino results in Super-Kamiokande-III", Phys. Rev. **D 83**, 052010, 2011

[35] H. Watanabe, et al., "First study of neutron tagging with a water Cherenkov detector", Astroparticle Physics **31**, 320–328 (2009).

[36] X. Dai, et al., "Wavelength shifters for water Cherenkov detectors", Nuclear Instruments and Methods in Physics Research **A 589,** 290–295 (2008).

[37] M. Sweany, et al., "Study of wavelength-shifting chemicals for use in large-scale water Cherenkov detectors", Nuclear Instruments and Methods in Physics Research **A 664**, 245–250 (2012).

[38] J. R. Alonso, et al., "Advanced Scintillator Detector Concept (ASDC): A Concept Paper on the Physics Potential of Water-Based Liquid Scintillator", arXiv:1409.5864v3 (2014).

[39] M. Yeh, et al., "A new water-based liquid scintillator and potential applications", Nuclear Instruments and Methods in Physics Research **A 660**, 51–56 (2011).

[40] M. Chen, "Potassium geo-neutrino detection", (2005). Available at http://www.docstoc.com/docs/82267645/Potassium-Geo-neutrino-Detection.

[41] P. Belli et al., "Development of enriched $^{106}CdWO_4$ crystal scintillator to search for double β decay processes in ^{106}Cd." Nuclear Instruments and Methods in Physics Research **A 615**, 301–306 (2010).

[42] B. Szczerbinska, "Potassium geoneutrino and their detection", Proceedings of the South Dakota Academy of Science **90**, 13 (2011).

[43] A. Drukier and L. Stodolsky, "Principles and applications of a neutral-current detector for neutrino physics and astronomy", Phys. Rev. **D 30**, 2295 (1984).

[44] M. Morita, "Theory of Beta Decay", Suppl.Progr.Theor.Phys., **No.26**, 1-63 (1963).

[45] C. Bisch, X. Mougeot, and M.-M. Bé, in 16th International Congress of Metrology, 07004 (2013).